Monthly Notices of the ROYAL ASTRONOMICAL SOCIETY

MNRAS **518,** L40–L44 (2023) https://doi.org/10.1093/mnrasl/slac127
Advance Access publication 2022 October 14

Flat-topped NIR profiles originating from an unmixed helium shell in the Type IIb SN 2020acat

K. Medler [1]★ P. A. Mazzali,[1,2] C. Ashall,[3] J. Teffs [1,4] M. Shahbandeh[5] and B. Shappee[6]

[1]*Astrophysical Research Institute, Liverpool John Moores University, Liverpool L3 5RF, UK*
[2]*Max-Planck Institute for Astrophysics, Karl-Schwarzschild-Str. 1, D-85748 Garching, Germany*
[3]*Department of Physics, Virginia Tech, Blacksburg, VA 24061, USA*
[4]*Areté Associates, 3194 N Swan Rd, Tucson, AZ 85712, USA*
[5]*Department of Physics, Florida State University, 77 Chieftan Way, Tallahassee, FL 32306, USA*
[6]*Institute for Astronomy, University of Hawai'i at Manoa, 2680 Woodlawn Dr., Hawai'i, HI 96822, USA*

Accepted 2022 October 7. Received 2022 October 7; in original form 2022 September 14

ABSTRACT

The Near Infrared (NIR) spectra of the Type IIb supernova (SN IIb) SN 2020acat, obtained at various times throughout the optical follow-up campaign, are presented here. The dominant He I 1.0830 and 2.0581 μm features are seen to develop flat-topped P-Cygni profiles as the NIR spectra evolve towards the nebular phase. The nature of the NIR helium peaks imply that there was a lack of mixing between the helium shell and the heavier inner ejecta in SN 2020acat. Analysis of the flat-top features showed that the boundary of the lower velocity of the helium shell was $\sim 3 - 4 \times 10^3$ km s^{-1}. The NIR spectra of SN 2020acat were compared to both SN 2008ax and SN 2011dh to determine the uniqueness of the flat-topped helium features. While SN 2011dh lacked a flat-topped NIR helium profile, SN 2008ax displayed NIR helium features that were very similar to those seen in SN 2020acat, suggesting that the flat-topped feature is not unique to SN 2020acat and may be the product of the progenitors structure.

Key words: supernovae: general-supernovae: SN 2020acat.

1 INTRODUCTION

Core-collapse supernovae (CC-SNe) result from high mass ($M > 8\,M_\odot$) stars that undergo rapid gravitational collapse. The structure of the stars outer hydrogen and helium envelops strongly influences the observational properties of the resulting SNe, creating several different types of CC-SNe (Matheson et al. 2001). One subcategory is the stripped envelope supernovae (SE-SNe), which are characterized by similar light-curve shapes, and spectra that display either weak or no hydrogen features (Clocchiatti & Wheeler 1997; Filippenko 1997). The presence of hydrogen within the outer envelope of SE-SN progenitors, with a hydrogen mass range of $M_H = 0.033$ to $1\,M_\odot$ (Hachinger et al. 2012; Gilkis & Arcavi 2022), results in a type IIb SN (SN IIb). These hydrogen rich SE-SNe are differentiated from the standard hydrogen rich CC-SNe by the transient nature of the hydrogen features within their spectra (Filippenko 2000). To achieve the thin hydrogen envelope required for SNe IIb, the outer envelope of the progenitor star must be stripped over the course of the stars evolution. Several proposed mechanisms can strip the outer envelope, including the transfer of mass from the progenitor to a companion star during a common envelope phase (Podsiadlowski, Joss & Hsu 1992) and the ejection of the outer layer by strong stellar winds during the Wolf–Rayet phase (Gräfener & Vink 2016). While both mechanisms may be able to explain the formation of SE-SNe, recent studies seem to favour binary over single star models (Smith et al. 2011).

Initially, the optical spectra of SNe IIb are dominated by P-Cygni profiles of hydrogen Balmer lines. These lines fade over time, as the photosphere recedes through the thin hydrogen envelope, and are replaced by He I lines (see, Filippenko 2000; Pastorello et al. 2008). Along with its optical lines, helium displays strong near-infrared (NIR) lines (Martin 1987) that dominate the NIR spectrum of SNe IIb (Shahbandeh et al. 2022). The NIR spectra provide vital information on the structure of the SN progenitor, especially the helium envelope. SNe IIb NIR spectra are dominated by the H I *Pa*, and the He I 1.0830 and 2.0581 μm lines (Shahbandeh et al. 2022). Although the H I *Pa* lines lie in a region heavily influenced by telluric effects, increasing the difficulty in obtaining clear observations. Despite this problem, both hydrogen and helium lines are expected to display P-Cygni profiles under the assumption of spherically expanding ejecta.

Here we present the NIR spectra of SN 2020acat obtained throughout the optical follow-up campaign (Medler et al. 2022). First in Section 2, we provide an overview on SN 2020acat and the results obtained from analysis of the photometry and optical spectra. In Section 3, we present the acquisition of the NIR spectra and discuss the evolution of the NIR spectra of SN 2020acat. In Section 4, we consider the presence and origin of flat-topped P-Cygni profiles seen within other SNe. In Section 5, we analyse the structure of the NIR helium features seen in SN 2020acat. Then in Section 6, we look at other SNe IIb NIR spectra to determine how unique the flat-topped helium structure is within other SNe IIb. Finally in Section 7, we present the conclusions from analysis of the NIR spectra of SN 2020acat and other SNe IIb.

★ E-mail: K.Medler@2019.ljmu.ac.uk

Table 1. Observational details for the NIR spectra of SN 2020acat. Phase is given from explosion date ($MJD_{exp} = 59192.01$) and given in rest frame. Air mass is the average airmass over the observation period.

UT date	MJD	Phase (d)	Instrument	Telluric STD	Airmass	Exposure (s)
24 − 12 − 2020	59207.66	15.53	NIRES	HIP54815	1.16	1200
23 − 02 − 2021	59268.33	75.72	NIRES	HIP54815	2.54	1200
22 − 04 − 2021	59326.33	133.27	NIRES	HD asdf	1.16	1200
24 − 05 − 2021	59358.34	165.02	NIRES	HD asdf	1.37	1200

2 SN 2020ACAT

SN 2020acat was a rapidly rising SN IIb caught within ∼1 d of explosion on 2020 December 9 ($MJD_{exp} = 59192.01$) at a redshift of $z = 0.0079$ (Medler et al. 2022). SN 2020acat underwent a thorough follow-up campaign with photometric observations ranging from the Ultra-Violet (UV) to NIR bands, along with comprehensive optical spectroscopic coverage. Analysis showed that SN 2020acat had a very fast rise time for a SNe IIb, reaching a bolometric peak of $L_{peak} = 3.09^{+1.28}_{-0.90} \times 10^{42}$ erg s^{-1} in 14.6 ± 0.3 d, approximately 4–5 d faster than typical SNe IIb. Medler et al. (2022) estimated that SN 2020acat had a ^{56}Ni mass of $M_{Ni} = 0.13 \pm 0.02$ M$_\odot$, along with an ejecta mass of $M_{ejc} = 2.3 \pm 0.3$ M$_\odot$, and a kinetic energy of $E_k = 1.2 \pm 0.2 \times 10^{51}$ erg. While the ejecta mass is average for SNe IIb, both the ^{56}Ni mass and the E_k produced by SN 2020acat are slightly larger (see Lyman et al. 2016; Prentice et al. 2019). The optical spectra of SN 2020acat initially displayed prominent hydrogen and helium lines, with a strong Hα signature lasting for ∼100 d. In the nebular phase, oxygen emission dominates over calcium. Finally, from analysis of photometry and spectra Medler et al. (2022) suggested that SN 2020acat originated from a compact progenitor with an initial mass of M_{ZAMS} between 15 and 20 M$_\odot$.

3 NIR SPECTRA

The NIR spectra of SN 2020acat were obtained using the Near-Infrared Echellette Spectrometer (NIRES: McLean et al. 1998) mounted on the 10 m Keck 2 telescope based at the W. M. Keck Observatory in Hawaii.[1] The NIR spectra were reduced using the reduction software SPEX[2] (Rayner et al. 2003; Cushing, Vacca & Rayner 2004) and were corrected for telluric effects using AV0 standard stars and the package XTELLCOR (Vacca, Cushing & Rayner 2003). Details on individual spectra are given in Table 1, with the phase given relative to the explosion date taken from Medler et al. (2022). The evolution of the NIR spectra of SN 2020acat is shown in Fig. 1, where all spectra have been corrected for redshift and normalized to the average continuum flux of the spectrum.

Initially, the day 15.53 spectrum displays a predominantly featureless continuum with only the hydrogen *Paβ* 1.2838 μm and He I 1.0830 μm and 2.0581 μm features visible. At this phase there is also a small noisy feature redwards of the He I 1.0830 μm peak. This is associated with the O I 1.1290 μm. As SN 2020acat evolves, features of heavier elements become more pronounced, with the O I 1.1290 μm, Ca II 1.1839 μm, and 1.1950 μm lines, along with the Mg I 1.1828 μm, 1.4878 μm, and 1.5033 μm lines, emerging in the day 75.72 spectrum. At this epoch the helium features start to transition from a smooth P-Cygni profile into a more flat-topped shape. Along with the change in shape, the two features develop a small peak-like feature just redwards of the emission wavelength. The presence of

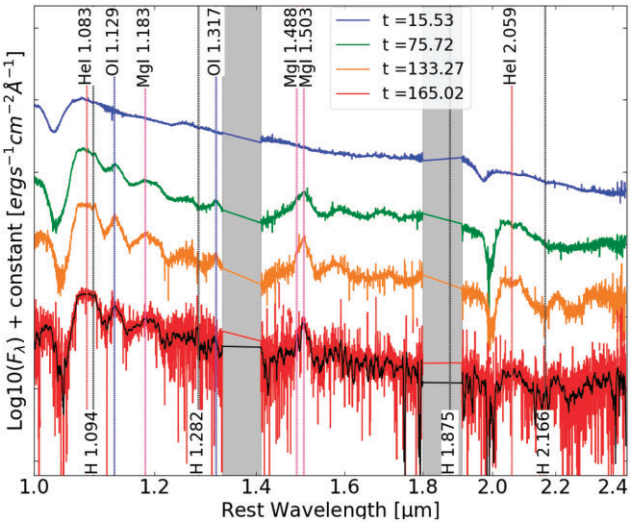

Figure 1. NIR spectroscopic evolution of SN 2020acat, corrected for redshift with telluric contamination (shaded regions) removed. The main emission lines are given by dashed lines. Phases are given relative to explosion date and given in rest frame. The black spectrum shows the smoothed day 165.02 spectrum, allowing a better view of spectral features.

these small peaks in both features dismisses the possibility that the peak by the He I 1.0830 μm line is the result of either the *Paγ* line or other elements. As the spectra evolve further, the O I 1.1290 μm and Mg I 1.5033 μm lines become narrower. By day 133.27 both helium features display a flat-topped profile, while continuing to exhibit the small red peaks. The He I 1.0830 μm peak exhibits a slight slope, declining from the blue edge of the flat-top, with the He I 2.0581 μm feature displaying a more symmetrical top centred on the rest wavelength of the emission line. At this epoch an additional feature emerges around 2.2 μm, which may be associated with the Na I 2.2090 μm line. Unfortunately the spectrum taken on day 165.02 had a very low signal-to-noise ratio (S/N), making the identification of any weak lines quite difficult. A Savitzky–Golay smoothing filter was applied to this spectrum using the python SCIPY (Virtanen et al. 2020) function savgol_filter,[3] which allowed the weaker features of the spectrum to be shown more clearly. As with the other late time spectra, clear features of He I 1.0830 and 2.0581 μm, O I, and Mg I were seen, along with the 2.2 μm feature.

4 FLAT-TOPPED P-CYGNI PROFILES

P-Cygni profiles are spectral features formed from the combination of a strong blueshifted absorption component, created by material moving towards the observer absorbing light originating from deeper within the material, and an emission peak around the emission wavelength, produced by the expanding ejecta moving in all directions (Fransson 1984). However, not all P-Cygni profiles display the symmetric emission peak centred around the rest wavelength of the line. Friesen et al. (2012) modelled the behaviour of resonance-scattering line profiles resulting in the development of both the commonly seen P-Cygni and a diversity of other line profile shapes. They found that the shape of the emission peak was strongly influenced by the optical depth of the emission region, with the flatter peaks emerging as optical depth was decreased. Flat-topped

[1] https://www.keckobservatory.org/
[2] http://www2.lowell.edu/users/massey/manual.pdf
[3] https://docs.scipy.org/doc/scipy/reference/generated/scipy.signal.savgol_filter.html

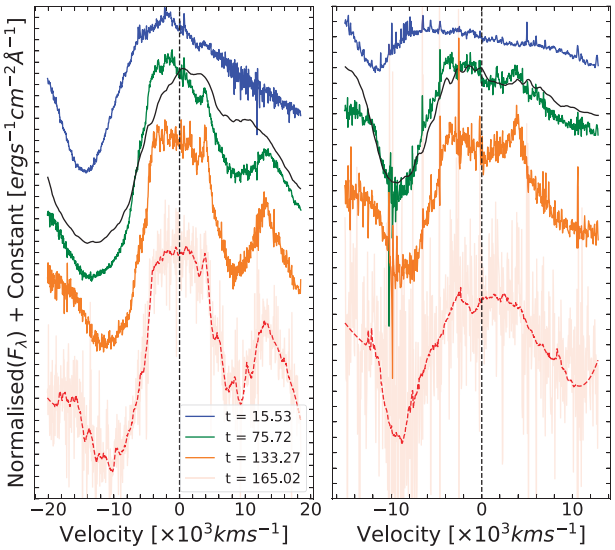

Figure 2. Velocity evolution of the He I 1.0830 and 2.0581 μm lines. Model fit to the day 75 spectrum (solid black line) shows a good fits the He I 2.0581 μm feature. The flat-top feature of the He I 1.0830 μm line develops the day 75 and 133 spectra, while the He I 1.0830 and 2.0581 μm line develops earlier between the day 15 and 75 spectra.

Table 2. Line velocity of the He I 1.0830 and 2.0581 μm lines derived from fitting the absorption minimum with a Gaussian fit. Associated errors obtained from fitting errors and noise within the spectra.

Phase (d)	He I 1.0830 μm velocity ($\times 10^3$ km s^{-1})	He I 2.0581 μm velocity ($\times 10^3$ km s^{-1})
15.53	14.4 ± 0.4	11.7 ± 0.5
75.72	13.3 ± 0.9	9.3 ± 1.0
133.27	11.4 ± 0.9	8.7 ± 0.9
165.02	10.7 ± 0.9	8.6 ± 3.6

P-Cygni profiles have been observed in the late time spectra of the Type II-pec SN 1987A (Bevan & Barlow 2015) and the NIR [Fe II] 1.257 and 1.644 μm lines of the Type Ia SN 2003hv (Motohara et al. 2006). In these cases, the flat-topped regions were associated with a low dust optical depth and a central region of iron-peak elements lacking enough ^{56}Ni to power the iron line emission, respectively. While the underlying physics of these flat-top regions may be similar, the physical conditions of each case are drastically different. The lack of ^{56}Ni rich ejecta associated with SN 2003hv is unlikely to cause the flat-topped profiles in SN 2020acat due to the drastically different explosion mechanisms of SNe Ia and SNe IIb. However, the physics of the flat-topped models described by Bevan & Barlow (2015), where there is a central region of low optical depth, may explain the shape of the helium NIR lines seen in SN 2020acat.

5 HELIUM 1.0830 AND 2.0581 μM FEATURES

Of all the NIR lines discussed in Section 3, the helium lines display the most drastic change as SN 2020acat evolves. The evolution of the He I 1.0830 and 2.0581 μm features is shown in Fig. 2, with the corresponding line velocity given in Table 2. In the earliest spectrum both helium features display broad P-Cygni profiles, as expected from spherically symmetric ejecta expanding at high velocity. The He I 1.0830 μm line displayed a faster overall velocity, falling from 14 400 to 10 700 km s^{-1}, compared to the He I 2.0581 μm line, which declined from 11 700 to 8600 km s^{-1}. It should be noted that the final velocity of the He I 2.0581 μm line has a much greater uncertainty compared to the other velocities due to the spectrum's very low S/N at this epoch. The He I 2.0581 μm line velocity declines rapidly between days 15.53 and 75.72, roughly twice the decline seen in the He I 1.0830 μm line velocity during this period. This is likely due to the weakness of the He I 2.0581 μm compared to the He I 1.0830 μm line. However, after the initial rapid decline the two line velocities continue to evolve at a similar pace.

Table 3. v_{edg} obtained from fitting the flat-topped He I 1.0830 and 2.0581 μm emission peaks.

Phase (d)	He I 1.0830 μm v_{edg} ($\times 10^3$ km s^{-1})	He I 2.0581 μm v_{edg} ($\times 10^3$ km s^{-1})
75.72	4.0 ± 0.5	3.9 ± 0.5
133.27	3.7 ± 0.5	3.9 ± 0.5
165.02	3.6 ± 1.0	3.6 ± 1.0

Along with the broad nature of the profiles, the initial spectrum's emission peaks are both blueshifted by several tenths of a micron with respect to the rest wavelength. As the spectrum evolves the peaks of the He I lines shift closer to their rest wavelengths and become flatter in shape. This is first seen clearly in the day 133.27 spectrum, where the features appear flat-topped with distinct cutoffs on either side of the lines' rest wavelength, and is still visible in the day 165.02 spectrum. The presence of a small peak just red of both He I lines is also interesting. We originally interpreted the feature red of the He I 1.0830 μm peak as resulting from the *Paγ* 1.094 μm line. However, a small peak is also seen near He I 2.0581 μm, at a similar displacement from the emission line, in a region with no associated hydrogen or heavy element emission lines. This strongly suggests that the small peaks are not due to different emission lines, and instead mark the start of the helium emission shell, placing a strong constraint on the lower limit of the helium shell velocity.

The day 75 spectrum was fit with a synthetic spectrum obtained using a modified version of the model described in Teffs et al. (2020), where helium was removed below a velocity of 5000 km s^{-1}. The synthetic spectrum was computed using our Montecarlo SN spectrum synthesis code (Mazzali & Lucy 1993; Lucy 1999; Mazzali 2000), including a non-thermal module for He I (Hachinger et al. 2012). The synthetic spectrum reproduced both the flat-topped P-Cygni profile of the NIR Helium features, shown in Fig. 2, and the standard P-Cygni profile observed in the optical spectra shown in Medler et al. (2022) at earlier times. While the synthetic spectrum reproduces the small red peak seen in both Helium lines, a feature expected as a result of a sharp inner cut-off of the helium shell, it fails to reproduce the He I 1.0830 μm feature in detail. This is likely caused by the contribution of other lines in this region (C I, Si II).

The widths of the flat-topped peaks were determined by fitting a Super-Gaussian function to the He I 1.0830 and 2.0581 μm peaks. The fit allows for the edges of the flat-top to be determined, while also fitting to the shape of the emission profile outside this region. It was assumed that the peaks are symmetrical around the rest wavelength once the flat-topped shape emerged. The edge velocities, v_{edg}, of the helium lines are given in Table 3, with errors arising from the fitting of the Gaussian and the S/N of the spectra. As SN 2020acat evolves, the width of the flat-top decreases as ejecta expand and the density of the emitting helium shell appears to decrease slightly, although this is within the measurement errors. The existence of a

minimum helium velocity indicates that the helium shell was not mixed down into the inner ejecta. To investigate the possibility of a non-mixed helium shell, we compared the velocity of the [O I] 6300, 6363 feature with the width of the flat-topped He I 1.0830 and 2.0581 μm features. This comparison allows for the boundary between the inner helium shell and the shell of oxygen-rich material to be probed. At both epochs the full-width half-maximum (FWHM) of the [O I] emission peak coincides with the v_{edg} of the helium shell to within ∼100 km s^{-1}(see Fig. 3). The lack of overlap between the helium and oxygen velocities strongly implies that the bulk of the two shells were not mixed prior to explosion.

6 SNE IIB HELIUM STRUCTURE

The flat-topped He I 1.0830 and 2.0581 μm features seen in the late time spectra of SN 2020acat imply a cut off to the helium shell at low velocity. The question arises whether this feature is unique to SN 2020acat or if it was seen in other SNe IIb. At early times ($t <$ 60 d), when the majority of NIR observations are obtained (Shahbandeh et al. 2022), SN 2020acat does not clearly show flat-topped helium features as the photosphere had not yet receded deep enough into the inner ejecta. As such, only SN 2008ax (Taubenberger et al. 2011) and SN 2011dh (Ergon et al. 2015) possess observations, with high enough S/N, to allow for good comparisons with SN 2020acat. The late-time He I 1.0830 and 2.0581 μm features of SN 2020acat are compared with those of SN 2008ax and SN 2011dh, obtained 11 − 06 − 2008 and 16 − 12 − 2011, respectively, in Fig. 4. It should be noted that the NIR spectrum of SN 2011dh does not extend to the He I 2.0581 μm line, so only SNe 2008ax and 2020acat are displayed in Fig. 4 (right-hand panel).

SN 2008ax seems to also display these narrow flat-topped NIR helium profiles, while SN 2011dh displays only a strong emission profile. When compared to SN 2020acat, the He I 1.0830 μm feature of SN 2008ax exhibits a more prominent slope along the top of the feature peaking at the blue edge of the flat-top. On the other hand, the He I 2.0581 μm line shows more of a symmetric double peak centred on the emission line, similar in nature to the line seen in the day 133.27 spectrum of SN 2020acat, although significantly narrower. It was initially suggested that the shape of the He I 1.0830 and 2.0581 μm lines in SN 2008ax may result from a non-uniform distribution of ^{56}Ni within the ejecta (Taubenberger et al. 2011). However, Maurer et al. (2010) suggested that the cause of flat-top shape seen in SN 2008ax was instead the result of a torus-shaped distribution of helium, along with an additional asymmetry along the line of sight to induce the strong blue peak seen in the He I 1.0830 μm line. Their models confined the majority of heavy elements to within the core with some mixing between the inner elements and the bottom of the helium shell.

The question remains what could cause the helium features to display flat-topped shapes in SNe 2008ax and 2020acat, but not in SN 2011dh. The flat-topped profiles may be explained by stellar evolution, where the He shell does not mix with the inner regions which have a much higher molecular weight. However, there are several possibilities that could give rise to flat-topped profiles, including asphericity in the explosion which could lead to element mixing in velocity space (e.g. Mazzali et al. 2005). The observed line profiles would then depend on the orientation of the line of sight. The small number of SNe IIb with late time NIR spectra, however, means that this suggestion is speculative in nature and requires a more extensive data set to determine its validity.

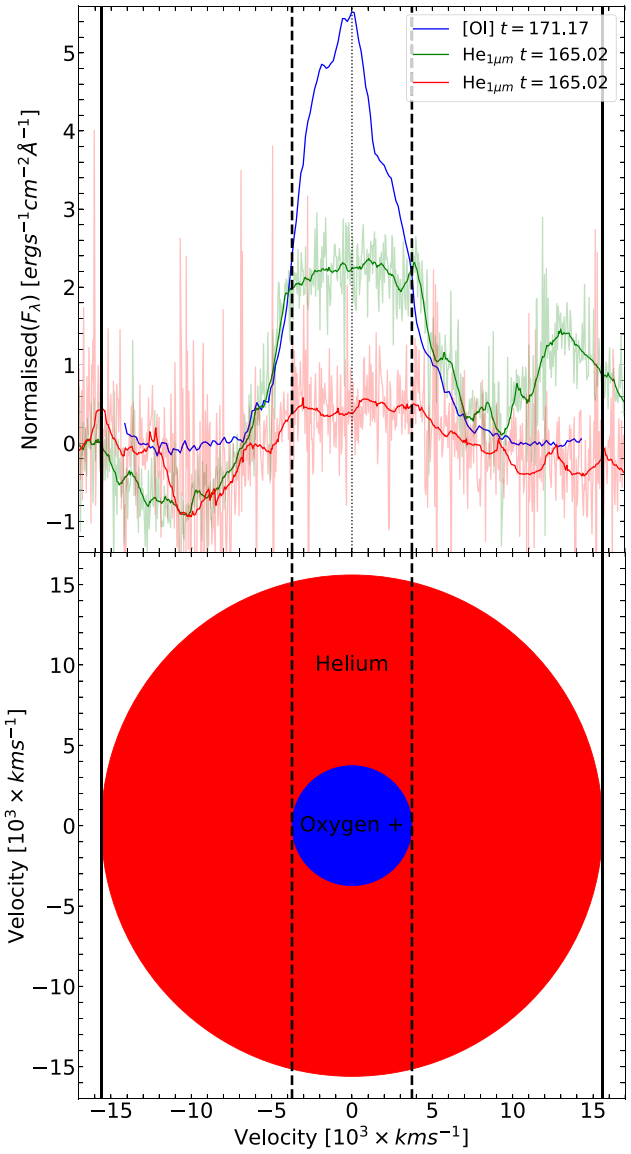

Figure 3. Top: Comparison of the late time [O I] 6300, 6363 peak and the smoothed NIR He I features. All features have been scaled to the continuum. The solid, dashed, and dotted vertical lines correspond to the Helium shell v_{edg}, the FWHM of the [O I] feature and the emission wavelength of each feature, respectively. Bottom: Structure of the helium and oxygen rich shells in SN 2020acat corresponding to the velocities derived from the spectra.

7 CONCLUSIONS

SN 2020acat displays interesting NIR spectra, which are dominated by the NIR helium lines and at later times display strong oxygen and magnesium lines. The He I features display a curious evolution, transitioning from a standard P-Cygni profile during the photospheric phase into a more flat-topped shape at late times. From the width of the two flat-topped peaks a lower limit on the velocity of the helium shell was obtained. Fitting the flat-top features revealed a minimum velocity of the helium shell of around ∼4.0 ± 0.5 × 10^3 km s^{-1}, which seem to slightly decline to a final velocity of ∼3.6 ± 1.0 × 10^3 km s^{-1} roughly 90 d later. The shape of these features are thought to originate from a lack of emitting helium within the ejecta material brought about by a low optical depth within the central region of the ejecta. Through a comparison with the [O I] 6300, 6363 emission

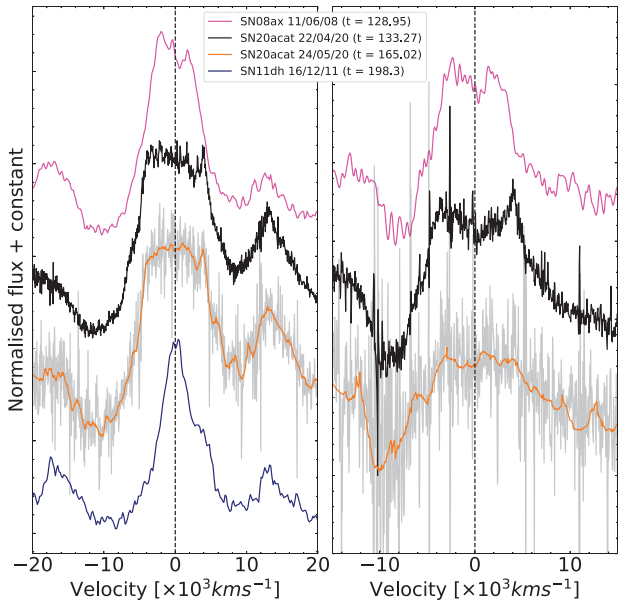

Figure 4. Comparison of the He I 1.0830 μm (left-hand panel) and the He I 2.0581 μm (right-hand panel) feature within the late time spectra of SN 2008ax (magenta), SN 2011dh (blue), and SN 2020acat (black and orange).

peak it was found that there is a lack of overlap between the helium and oxygen features, strongly suggesting that there is little or no mixing between the helium and oxygen-rich shells.

Once the flat-topped helium features were identified, a comparison with other SNe IIb NIR spectra was done to determine if the features were unique to SN 2020acat. Due to the lack of late-time NIR observations for SNe IIb, only SN 2008ax and SN 2011dh possessed spectra that could be compared with SN 2020acat. While SN 2008ax displayed a similar flat-topped feature, although significantly smaller in width, SN 2011dh displayed a sharp emission profile expected for spherically symmetric ejecta. A non-spherically shaped helium shell is likely to be the origin for the flat-topped profile seen in SN 2008ax and SN 2020acat, which may be linked to the structure of their progenitors. If the feature is indeed linked to the nature of the SNe progenitor, it may be used to determine the structure of the progenitor of events with limited observations, so long as late time NIR spectra are obtained. However, due to the limited number of SE-SNe NIR spectra, a larger sample of NIR spectra is currently needed to confirm the connection between progenitor structure and shape of the NIR helium feature.

ACKNOWLEDGEMENTS

KM is supported by Science and Technology Facility Council (STFC) grant ST/T506278/1. BJS is supported by National Science Foundation (NSF) grants AST-1920392 and AST-1911074.

DATA AVAILABILITY

Spectral data is available on the Weizmann Interactive Supernova Data Repository (WISeREP) at https://wiserep.weizmann.ac.il/.

REFERENCES

Bevan A., Barlow M. J., 2015, MNRAS, 456, 1269
Clocchiatti A., Wheeler J. C., 1997, ApJ, 491, 375
Cushing M. C., Vacca W. D., Rayner J. T., 2004, PASP, 116, 362
Ergon M. et al., 2015, A&A, 580, A142
Filippenko A. V., 1997, ARA&A, 35, 309
Filippenko A., 2000, in Zhang W. W., Holt S. S., eds, AIP Conf. Proc. Vol. 522, Cosmic Explosions: Tenth Astrophysics Conference. Am. Inst. Phys., New York, p. 123
Fransson C., 1984, A&A, 132, 115
Friesen B., Baron E., Branch D., Chen B., Parrent J. T., Thomas R. C., 2012, ApJS, 203, 12
Gilkis A., Arcavi I., 2022, MNRAS, 511, 691
Gräfener G., Vink J. S., 2016, MNRAS, 455, 112
Hachinger S., Mazzali P. A., Taubenberger S., Hillebrandt W., Nomoto K., Sauer D. N., 2012, MNRAS, 422, 70
Lucy L. B., 1999, A&A, 344, 282
Lyman J. D., Bersier D., James P. A., Mazzali P. A., Eldridge J. J., Fraser M., Pian E., 2016, MNRAS, 457, 328
Martin W. C., 1987, Phys. Rev. A, 36, 3575
Matheson T., Filippenko A. V., Li W., Leonard D. C., Shields J. C., 2001, AJ, 121, 1648
Maurer I., Mazzali P. A., Taubenberger S., Hachinger S., 2010, MNRAS, 409, 1441
Mazzali P. A., 2000, A&A, 363, 705
Mazzali P. A., Lucy L. B., 1993, A&A, 279, 447
Mazzali P. A. et al., 2005, Science, 308, 1284
McLean I. S. et al., 1998, in Fowler A. M., ed., Proc. SPIE Conf. Ser. Vol. 3354, Infrared Astronomical Instrumentation. SPIE, Bellingham, p. 566
Medler K. et al., 2022, MNRAS, 513, 5540
Motohara K. et al., 2006, ApJ, 652, L101
Pastorello A. et al., 2008, MNRAS, 389, 955
Podsiadlowski P., Joss P. C., Hsu J. J. L., 1992, ApJ, 391, 246
Prentice S. J. et al., 2019, MNRAS, 485, 1559
Rayner J. T., Toomey D. W., Onaka P. M., Denault A. J., Stahlberger W. E., Vacca W. D., Cushing M. C., Wang S., 2003, PASP, 115, 362
Shahbandeh M. et al., 2022, ApJ, 925, 175
Smith N., Li W., Filippenko Alexei V., Chornock R., 2011, MNRAS, 412, 1522
Taubenberger S. et al., 2011, MNRAS, 413, 2140
Teffs J., Ertl T., Mazzali P., Hachinger S., Janka T., 2020, MNRAS, 492, 4369
Vacca W. D., Cushing M. C., Rayner J. T., 2003, PASP, 115, 389
Virtanen P. et al., 2020, Nat. Methods, 17, 261

This paper has been typeset from a TEX/LATEX file prepared by the author.